Influence of layer interface geometry on single-layer folding

Albert Griera[1*], Enrique Gomez-Rivas[2,3] and Maria-Gema Llorens[1]

1) *Departament de Geologia, Universitat Autònoma de Barcelona, 08193 Bellaterra (Cerdanyola del Vallès), Spain*
2) *Departament de Mineralogia, Petrologia i Geologia Aplicada, Facultat de Ciències de la Terra, Universitat de Barcelona, 08028 Barcelona, Spain*
3) *School of Geosciences, King's College, University of Aberdeen, Aberdeen AB24 3UE, United Kingdom*
   [*]*Corresponding author. Tel: +34-935811035; Fax: +34-935811263; E-mail address: albert.griera@uab.cat*

Abstract: Geometrical heterogeneities along layer interfaces play a key role to determine the geometries of folds developed during shortening of competent layers. We present a series of numerical simulations to investigate the influence of initial sinusoidal perturbations on folding of single layers. Models consist of a competent viscous single layer embedded in a softer matrix, with the layer oriented parallel to the shortening direction. We first generalise the wide spectrum of sinusoidal perturbations accounting for asymmetries along and across a competent single-layer, using two parameters: transversal asymmetry (A') and longitudinal asymmetry (φ). These two parameters allow studying a transition between classical fold shape and pinch-and-swell geometries. The parameter A' describes the development of fold hinges with different geometries between upper and lower layer interfaces and abnormal curvatures between outer and inner arcs of fold hinges. The parameter φ induces a strong polarity on folds, with systematic preferred orientation of the pinch and swell regions of the layer, even if there is no shear component parallel to the layer. Our results demonstrate the importance of structural inheritance on the resulting fold geometries and suggest that caution must be taken when using certain types of asymmetric folds as strain markers and kinematic indicators.

Keywords: folding, structural inheritance, geometrical heterogeneities, asymmetric folds, fold shapes

Folds form when stiff or competent viscous layers get shortened. Folds are observable across all length scales in orogenic belts (from micro- to kilometre scales), and are widely used as kinematic and mechanic indicators (*e.g.*, Hudleston and Treagus, 2010; Llorens et al., 2013a; 2013b; Schmalholz and Mancktelow, 2016). To commemorate the 50 anniversary of the publication of "Folding and fracturing of rocks" by John Ramsay (Ramsay, 1967), here we focus on how pre-existing interface geometries of folding layers affect fold formation. Ramsay and Huber (1987) discussed in their book the so-called "fish-hook" folds (Fig. 1; and see their Fig. 17.11). Initially described by Sorby (1879), and discussed in Ramsay and Huber (1987), the train of fish-hook folds is observed in a bioclastic crinoidal limestone embedded in slates. The structure is characterised by a marked fold polarity (or asymmetry), with large differences in thickness between consecutive limbs and also with marked hinge geometry variations along the upper and lower layer interfaces (Fig. 1). Cleavage is well developed in this classical example and gets refracted in the limestone single-layer, indicating a more competent behaviour than that of the host slates.
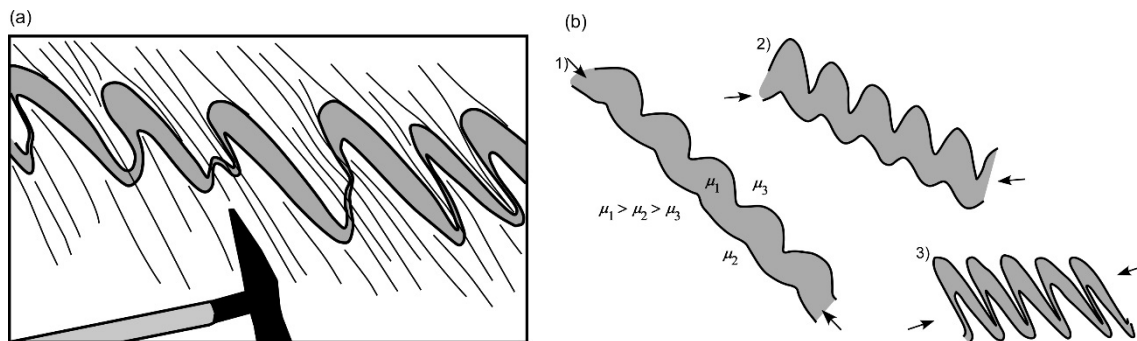

Figure 1. (a) Sketch of the "fish-hook" folds of Ramsay and Huber (1987). Note the marked asymmetry of folds and differences on geometry between hinges located at the upper and lower layer interfaces. Thin lines indicate foliation. (b) Deformation sequence suggested by Ramsay and Huber (1987). The layer is embedded in matrices with different viscosities ($\mu_1 > \mu_2 > \mu_3$). There is a distinct wavelength selection along interfaces during shortening. Progressive rotation of the shortening direction with respect to the layer produces the fold asymmetry. Arrows indicate the incremental shortening directions.

An issue when interpreting this type of structure is how to explain fold polarity. Ramsay and Huber (1987) wrote that they were not able to provide a confident explanation of this structure, but suggested a way of interpreting it based on a tri-layer system, in which the incompetent host rock above and below the competent folding layer have different viscosities. They concluded that the only satisfactory explanation of the polarity of the structure was that the initial perturbations already presented this polarity, and suggested that such geometry would arise from competence differences of the two sides of the folding layer (Fig. 1b, stage 1). During non-coaxial deformation the viscosity contrast between host rock and folding layer induces a distinct wavelength selection along the upper and lower interfaces of the layer (Fig. 1b, stage 2), and the progressive rotation of the principal shortening axis with respect to the layer causes the fold asymmetry and the preferential thinning of one of the fold limbs (Fig. 1g, stage 3).

Ramsay and Huber (1987) assumed that the original thickness of the layer was uniform, and that thickness variations were developed during deformation. In terms of fold perturbation, the explanation they proposed implies an asymmetry on amplitude of perturbations developed on the upper and lower interfaces of the competent layer, resulting in an asymmetry transversal to the layer. Additionally, although not represented in the figures of Ramsay and Huber (1987), the selected wavelengths could be different

2

along both interfaces, and the fold hinges at one of the interfaces did not match the location of the corresponding one at the other interface. This condition results in the development of a longitudinal asymmetry parallel to the layer. Recent thoughtful reviews summarise the information that can be obtained from fold analysis (*e.g.*, Hudleston and Treagus 2010), as well as the fundamental parameters controlling folding (*e.g.*, Schmalholz and Mancktelow 2016). However, most of the existing studies on folding have only considered folds developed from perturbations defined by regular arrays of low-amplitude and symmetric geometries, and the influence of irregular and/or inherited perturbations was not addressed, although geometrical heterogeneous folds are abundant at field (Fig. 2a-c). Assuming that certain fold types, such as "fish-hook" folds, originate from inherited layer perturbations, the geometries of perturbations along and across the folding layer have to be clearly defined. This contribution presents an investigation of the influence of initial asymmetries along and across a competent single-layer embedded in a ductile matrix during layer-parallel shortening. This is systematically studied by means of numerical simulations. We first define the parameters used to generalise sinusoidal perturbations accounting for asymmetries along and across a competent single-layer. These variations are described using two parameters that measure the degree of asymmetry along and across to the layer envelope. After a preliminary analysis of the problem using the analytical theory of folding, the finite evolution of the structures nucleated from these perturbations is systematically explored using a series of numerical simulations that considers viscous rheology. Finally, the main implications of our results on the use of folds structures as strain and kinematic indicators are discussed.

Layer interface geometry

The occurrence of small and regular/random irregularities on layer interfaces is assumed in all theories of single-layer folding (*e.g.*, Biot 1957, 1961; Ramberg, 1960; Fletcher 1974, 1991; Smith, 1975, 1977, 1979; Schmalholz and Podladchikov, 2000). Finite wavelength, amplitude and shape of evolved folds are strongly influenced by the initial geometry of these perturbations (Abassi and Mancktelow, 1990; Mancktelow, 1999), and have been investigated by means of analogue experiments (Cobbold, 1975; Abassi and Mancktelow, 1990, 1992) as well as numerical simulations (Williams et al. 1978; Mancktelow, 1999; Zhang et al. 1996, 2000). However, these studies have only considered single layers of constant thickness defined by regular arrays of low-amplitude perturbations and symmetric shapes. Results from experiments of Williams and Jiang (2001, see their figs. 2 and 7) on single-layer folding using rock analogue materials show the strong influence of initial irregularities during folding. Large variations on fold structures were observed in their experiments, although the samples were deformed using the same configuration, materials and deformation conditions. Following a kinematic study, they interpreted that slight differences on the relative geometry between both layer interfaces can produce high deviations of the nucleated and amplified structures during layer-parallel shortening.

Smith (1975, 1977) defined four main types of structures that can grow from deformation of a single-layer embedded in a matrix, depending on (1) the viscous contrast between layer and matrix and (2) whether layer is subjected to shortening or lengthening. When a single layer experiences shortening folds or mullions are expected to develop if the layer is stiffer (folds) or weaker (mullions) than the matrix. Additionally, when the layer is subjected to parallel extension, pinch-and-swell structures (or necking) are

expected to form if the layer is stiffer than the matrix, while reverse folding structures develop if the layer is weaker than the matrix.
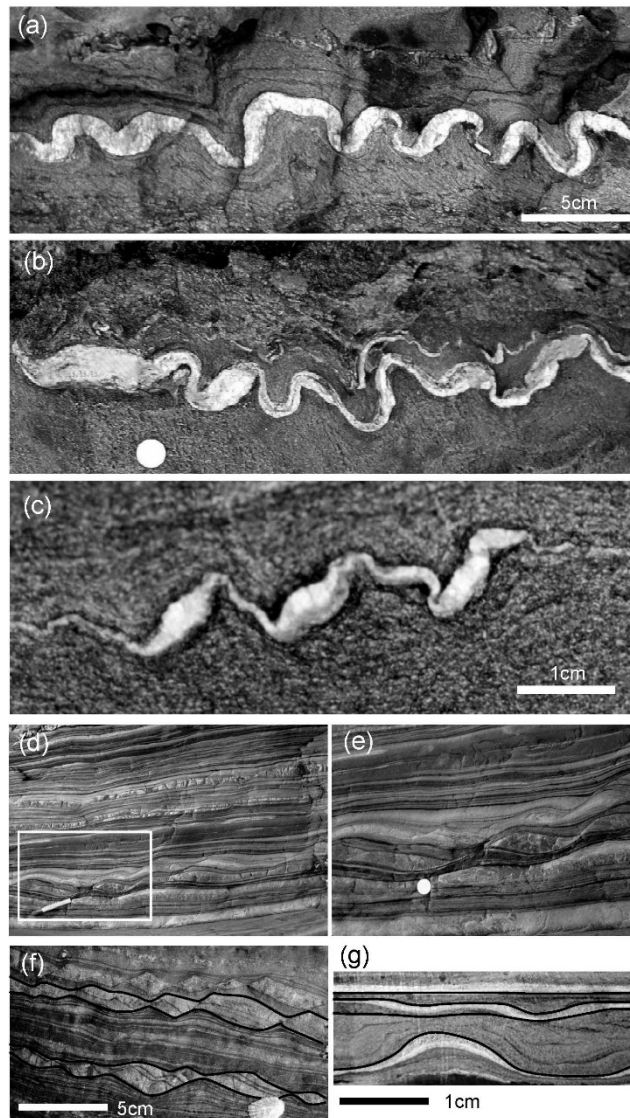

Figure 2. (a to c) Folded quartz veins with highly irregular geometries from the Variscan Belt of Cap de Creus (NE Spain). The structure is interpreted to have formed as a result of folding of initial pinch-and-swell structures or a layer with strong thickness variation. (d to f) Natural examples of geometrical heterogeneities along layers at Gabieira beach (NW Spain). (d) Example of shear boundins. Note the deviation of the fold arcs between upper and lower layer interfaces. The square box indicates the enlarged area of figure (e). (f) Example of asymmetric boudins. Black lines indicate layer interfaces. (g) Natural example of siltstone layers embedded in anhydrite/halite layers (white layers) displaying irregular bedding and heterogenous thickness at the Súria anticline (NE Spain).

From a geometrical point of view, these four structures can arise from two basic initial layer interface perturbation geometries (Fig. 3c): (a) symmetric, when the perturbation is mirrored both along the layer and normal to it (*i.e.*, with a "pinch-and-swell" or "neck" shape) and (b) antisymmetric, when the perturbation is only mirrored normal to the plane but not parallel to it (*i.e.*, resulting in a deflection or "fold" shape). Although these perturbations can reflect different deformation conditions not considered here, from a geometrical point of view these geometries can be regarded as the end members of a progressive transition between "fold" and "pinch-and-swell" shapes (Fig. 3a). This has been explicitly taken in account in several numerical and experimental

4

studies, in which mullion structures were modelled using both symmetric and antisymmetric perturbations (Sokoutis, 1987, 1990; Lan and Hudleston, 1991).

In general, layers in natural rocks are likely to deviate from perfectly planar geometries and tend to contain random irregularities along layer interfaces as well as lateral variations of layer thickness (Fig. 2d-g). These irregularities can sometimes be systematic as result of primary structures (*e.g.*, sedimentary cross-bedding, lenticular bed geometries, irregular igneous dykes, etc.). Other times, a new deformation phase is superposed to previously deformed materials resulting in the formation of arrays of periodic and/or random layer interface irregularities, as for example, pinch-and-swell structures or asymmetric boudinage (Fig. 2d-f). However, most of the published experimental and numerical studies only focused on layers with planar geometries, initial symmetric layer interface perturbations or those characterised by very small random irregularities. However, non-systematic perturbations are expected across and along layer interfaces in the vast majority of natural rocks.
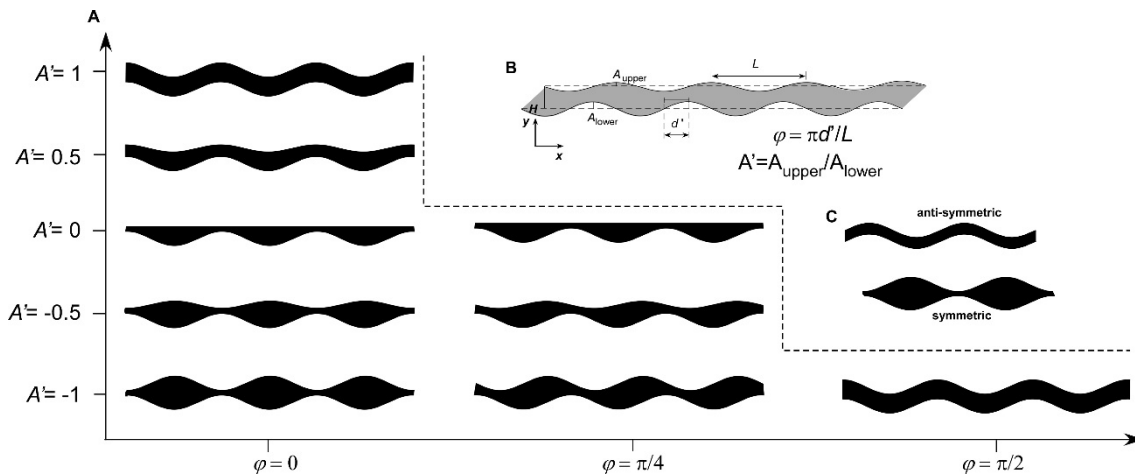

Figure 3. (a) Variation of the initial fold perturbation as a function of the transversal (*A'*) and longitudinal asymmetry (*φ*). Note that there is a progressive transition between the two end-member geometries (symmetric and antisymmetric). (b) Definition of the main parameters used to describe the geometry of perturbations. *L* and *H* are the layer wavelength and thickness, A_{lower} and A_{upper} are the amplitude of lower and upper interfaces and *d'* is the distance between arcs at the upper and lower interfaces. (c) Geometry of an antisymmetric (fold shape) and symmetric (boudin or pinch-and-swell shape) perturbations. In all the sketches the amplitude of irregularities is exaggerated to facilitate the visibility of the geometries.

Generalisation of the perturbation geometry

Prior to presenting and discussing the series of numerical simulations, here we present a generalisation of the perturbation geometry. Similarly to classical fold theories (*e.g.*, Biot 1957, 1961; Ramberg, 1960; Fletcher 1974, 1991; Smith, 1975, 1977, 1979; Schmalholz and Podladchikov, 2000), a regular and sinusoidal shape of perturbations is considered. Assuming an initial flat layer parallel to the reference *x*-axis, the geometry *ζ(x)* of perturbations along the upper interface of a layer can be described as:

$$\zeta_{upper}(x) = H/2 + A_{upper}\cos(\frac{2\pi}{L}x) \tag{1}$$

where *H* is the layer thickness, *A* is the amplitude and *L* the wavelength of the perturbation (Fig. 3b). A similar expression can be used to define the geometry of the lower interface:

$$\zeta_{lower}(x) = -H/2 \pm A_{lower} \cos(\frac{2\pi}{L}x) \qquad (2)$$

If the amplitude of both interfaces has the same sign the shape of the perturbation is antisymmetric (Fig. 3c). Contrarily, if the amplitudes of the two interfaces have different signs then the shape of the perturbation is symmetric. The variation between both end-members can be described using a normalised parameter A', namely transversal asymmetry. A' is defined as the ratio between the amplitude of the upper and lower interfaces, $A'=A_{upper}/A_{lower}$. The geometry of the perturbation is antisymmetric for $A'=1$, while $A'=-1$ denotes the case of symmetric configuration (Fig. 3b). Values of A' ranging from -1 and $+1$ define geometries in between the two end members. $A'=0$ is a particular case in which one of the interfaces is planar.

In addition to the asymmetry of perturbations across the layer, asymmetries along the layer can also be defined. If we consider trains of sinusoidal perturbations with constant wavelength, an additional term can be added to describe the relative shift between hinges of upper and lower interfaces. This parameter, namely longitudinal asymmetry (φ), can be expressed as:

$$\varphi = \pi\frac{d'}{L} \qquad (3)$$

where d' is the distance between consecutive maximum and minimum amplitudes of the lower and the upper interfaces, respectively (Fig. 3b). Note that this definition is similar to the one used for expressing the phase difference between two sinusoidal waves with the same wavelength. Using Eq. 3, $\varphi=\pi/2$ describes a train of sinusoidal perturbations with an antisymmetric geometry (Fig. 3a, $A'=-1$ and $\varphi=\pi/2$), while $\varphi=0$ denotes a symmetric geometry (Fig. 3a, $A'=-1$ and $\varphi=0$). Values between the two end members ($\varphi \in [0, \pi/2]$) are equivalent to perturbations that display geometries similar those of asymmetric boudins or shear bands (*e.g.*, Goscombe and Passchier, 2003; Swanson, 1992). Although the treatment is different, a value of $\varphi \approx \pi/2$ yields similar geometries those used in the analogue experiments of Abassi and Mancktelow (1990).

Using the transversal and longitudinal asymmetry parameters, eq. (1) can be rewritten as,

$$\zeta_{upper}(x) = \frac{H}{2} + (A'A_{lower})\cos\left(\frac{2\pi}{L}x + \varphi\right) \qquad (4)$$

Sinusoidal perturbations with asymmetries along and across the layer (*i.e.*, in the x and y direction, respectively) can be defined using both parameters. The range of explored values is limited to $A' \in [-1,1]$ and $\varphi \in [0,\pi/2]$ in this study.

In this contribution, the term boudin is used to describe the swell region of the layer (*i.e.*, where the layer thickness reaches a maximum), whereas the term neck describes the pinch part of the layer. Note that these terms do not imply a mechanical interpretation of the origin of these perturbations and are only used to describe layer geometries. From a physical point of view, these ideal perturbations let us explore the influence of the layer thickness variation and the effect of non-coincident hinge/inflection points on fold geometries.

Analytical solution

The classical theory of folding of linear viscous layers is based on the studies of Biot (1959; 1961) and Ramberg (1960). Later on, other authors modified the theory to include

non-linear rheologies (Fletcher, 1974; Smith 1975, 1977) or extended it for the three-dimensional case (Fletcher, 1991, 1995; James and Watkinson 1994). However, these analytical studies are restricted to infinitesimal-amplitude solutions and perturbations with simple sinusoidal geometries. Remarkably, Schmaholz and Podladchikov (1999; 2000) proposed a new finite amplitude theory of folding that overcomes these restrictions and provides results that match those obtained from numerical simulations (Schmaholz and Podladchikov, 2001). A useful review of theoretical studies and analytical solutions for single-layer folding is provided by Schmalholz and Mancktelow (2016).

For a two-dimensional system, the rate of amplification of an infinitesimal perturbation in a linear viscous medium is given by (e.g. Schmalholz and Mancktelow, 2016),

$$\frac{dA}{dt}\frac{1}{A} = -(1+q)\dot{\varepsilon}_{xx} \tag{5}$$

where A is the amplitude, t is the time and $\dot{\varepsilon}_{xx}$ is the bulk layer-parallel strain rate shortening. The term in parentheses, a dimensionless or dynamic growth rate q, corresponds to the amplification due to passive growth rate. According to Johnson and Fletcher (1994), the infinitesimal amplitude solution for q can be expressed as:

$$q = \frac{8k(1-m)m}{4k(m^2-1) \pm (m+1)^2 e^{2k} \mp (m-1)^2 e^{-2k}} \tag{6}$$

where m is the viscosity contrast between the layer and matrix (η_l / η_m), and k is the wavenumber (i.e., $\pi H/L$). For layer-parallel shortening, Smith (1975; 1977) demonstrated that the expression of q is similar for both symmetric and antisymmetric perturbation cases. The difference between the two of them is the change of signs of the terms in the quotient of eq. (6). Upper signs are used for symmetric cases, while lower signs refer to asymmetric ones. The sum of the kinematic (i.e., passive amplification) and dynamic growth rates (1+q) is plotted against L/H for both types of perturbations in Fig. 3. For the antisymmetric case, the dynamic growth rate is higher than the kinematic amplification and thus the perturbation is amplified. In such a scenario, the amplification rate follows an exponential growth rate (Biot, 1961; Ramberg, 1960) but quickly changes to a non-linear growth rate related to the finite amplitude of folding (see Schmalholz and Podladchikov, 2000). For symmetric cases, dynamic growth rates q are negative and, therefore, the predicted amplification is lower than the kinematic amplification due to homogenous deformation. For a constant viscosity contrast, the curves obtained for the antisymmetric and symmetric perturbation cases constrain the maximum and minimum values of the amplification fold growth rate spectra. Note that the maximum and minimum amplification rates occur at the same L/H and are coincident with the dominant wavelength to thickness ratio (L_d/H). For these cases, the dominant wavelength is $L_d = 2\pi H(m/6)^{1/3}$. General perturbations are expected to have growth rates ranging between these limits, as shown in Fig. 4.

Burg et al (2004) defined an analytical solution for the growth rate of a folding layer with planar interface (i.e., $A'=0$). The dynamic growth rate q can be expressed as follows, based on Eq. 8 of Burg et al (2004) and assuming folding in the absence of gravity:

$$q = \frac{6k\mu_l}{4\mu_l k^3 + 3\mu_m} \tag{7}$$

The dominant wavelength is $Ld = 2\pi H(m/3)^{1/3}$ in this situation. Note that for the case with a flat interface, the growth rate decreases, while the dominant wavelength increases with respect to the previous scenario with antisymmetric perturbation (Fig. 4). For a hypothetical case with $m=100$, the dominant wavelength is $L_d/H=16$ for the antisymmetric

perturbation case, while for the example with a planar interface it is $L_d/H=20$, slightly larger. For the cases with $1<A'<0$, the growth rates are expected to be essentially very similar (Fig. 4). However, the expected range of growth rates is larger in models with $A'<0$. An analytical solution of the growth rate using stability analysis is not available for the case of longitudinal asymmetries φ.
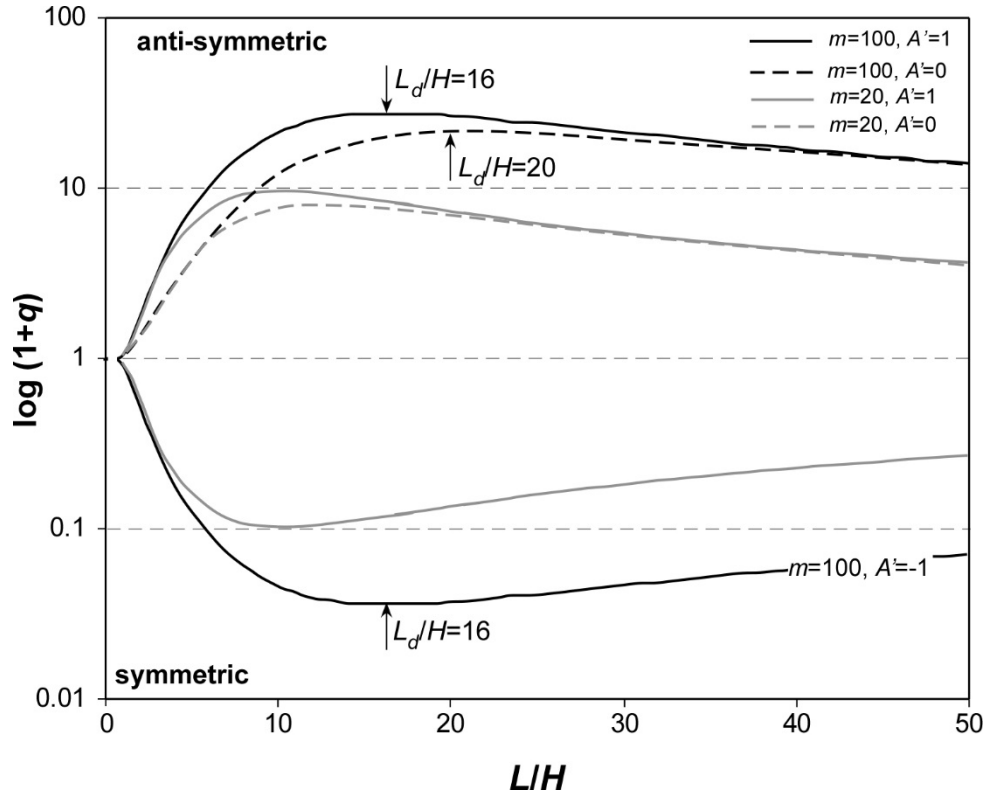

Figure 4. Logarithmic of the dimensionless amplification rate $(1+q)$ *vs.* wavelength to thickness ratio (L/H) for linear viscous folding, for viscosity ratios of $m=20$ (grey curves) and $m=100$ (black curves). The curves correspond to the cases with a symmetric ($A'=-1$), antisymmetric ($A'=1$) and with one flat interface ($A'=0$), respectively. Decreasing A' reduces the dimensionless amplification rate. Note that for the symmetric and antisymmetric cases the dominant wavelength to thickness ratio (L_d/H) is the same, but for $A'=0$ L_d/H is higher.

The analytical solution of Burg et al. (2004) is based on a linear first-order approximation and is only valid for gentle and infinitesimal-amplitude perturbations. Therefore, this solution cannot be used to predict the finite evolution of folds. As mentioned above, Schmaholz and Podladchikov (1999; 2000) proposed a new finite amplitude theory of folding that overcomes these restrictions and provides results coherent with numerical simulations (Schmaholz and Podladchikov, 2001). However, the present problem cannot be simplified to the study of only one of the interfaces, because there are differences in amplitudes and shifts of hinge/inflection points across the layer. This can potentially imply hinge migration and non-homogenous distribution of shear stress across and along the layer, at least at low deformation stages. Schmalholz et al. (2008) obtained an analytical solution for finite amplitude necking based on the assumption that plane sections remain plane (PSRP). This approach can potentially be used to predict the finite evolution of asymmetric perturbations because can handle large lateral variations of layer thickness. However, this is beyond the scope of this paper and the problem is treated here by means of numerical simulations.

Methods and model setup

Numerical Method

The numerical simulations have been performed using the 2D finite difference program FLAC (Cundall and Board, 1988; Itasca, 1998). The equations of motion in a continuum medium are discretized and solved using a dynamic relaxation scheme (Cundall and Board, 1988). The medium is simulated using a structured mesh composed of four-node polyhedral elements, where a mixed discretisation scheme is used for the handling of volumetric constraints. Both schemes (i.e. dynamic relaxation and mixed discretisation) provide an efficient strategy and robustness in modelling strain localisation (Poliakov and Hermann, 1994). The code has been widely used to simulate layer folding (*e.g.*, Zhang et al., 1996; Zhang et al., 2000; Toimil and Griera, 2007) and other tectonic structures (Takeda and Griera, 2006 and references therein).

Model geometry and boundary conditions

The geometry of the model consisted of a competent layer embedded in a weaker matrix. The thickness of the layer is 2 units, the model length 80 units and the width 44 units. Following other studies based on single-layer folding simulation (*e.g.*, Zhang et al. 1996, 2000; Mancktelow, 1999), the contacts between layer and matrix are considered coherent or "welded", *i.e.* without the possibility of slipping and/or opening. Between 2,880 and 3,520 quadratic elements are utilised and the mesh is progressively refined around the layer/matrix contact. A total of six elements are used to represent the layer width. This resolution is high enough for a correct distribution of stress and strain inside and around the layer. All the models are deformed under coaxial plane strain conditions with a constant strain rate of $2.5 \cdot 10^{-14}$ s^{-1}. Progressive shortening parallel to the layer is imposed by velocity boundary conditions applied to the sides of the model. Velocities normal to the sides are fixed, while parallel velocities are not constrained (i.e free slip boundary conditions). The maximum shortening applied in all models was 55%, equivalent to a natural strain $\varepsilon=0.8$.

Two basic perturbation configurations were used: (a) models with periodic small perturbations (i.e. constant wavelength and amplitude) and (b) models with a single isolated perturbation located at the centre of the layer. These configurations can be considered equivalent, but not similar, to previous models used by other authors in their numerical simulations (*e.g.*, Williams et al. 1978; Zhang et al. 1996, 2000; Mancktelow, 1999). The geometry of these perturbations has been defined using the equations (1) and (3). For models with periodic perturbation, the maximum amplitude (i.e. hinge) of the perturbations coincides with the model boundaries (i.e. hinge point at boundary). Additionally, periodic boundary conditions in *x*–direction are imposed to minimize boundary effects, using an approach than that of the ELLE platform (*e.g.*, Jessell et al., 2009; Llorens et al., 2013a; 2013b; Gomez-Rivas et al., 2017). For all models, the geometry of the upper interface is kept constant and is defined by an initial *L/H*=20 and *A/H*=0.2, while the geometry of lower interfaces varies according the values of *A'* and *φ*.

Material properties

A linear elastoviscous model is used to describe the material rheology. This constitutive model is equivalent to a combination of a linear elastic element and a linear viscous

element in series following a Maxwell model (*e.g.*, see Ranalli, 1987). The total strain rate is assumed to be the sum of the elastic and viscous strain rates. The elastoviscous properties of the material have been defined using the shear modulus (G), the bulk (or incompressibility) modulus (K) and the shear viscosity (η) of the material. A Poisson's ratio (v) of 0.30 is assumed for both the folding layer and the matrix. In all the simulations, volumetric strain is considered purely elastic. Materials properties are summarised in table 1. These values are within the range inferred from experiments of natural rocks in ductile conditions (Turcotte and Schubert, 1982) and similar to those utilised by other authors (*e.g.*, Mancktelow, 1999; Zhang et al., 2000).

For elastoviscous materials, important material parameters are the contrast of elasticity (R) and viscosity (m) between the folding layer and matrix (Zhang et al., 2000). Here, we have opted to follow an approach where both parameters are independent, rather than using similar values for both parameters (*i.e.*, $R=m$). This assumption is coherent because viscosity in natural rocks ranges up to four orders of magnitude (e.g. Carter and Tsenn, 1987), while the ratio of elastic properties is only up to one order (e.g. Turcotte and Schubert, 1982; Mancktelow, 1999). For all numerical simulations an elastic contrast $R=2$ and viscosity contrast $m=20$ were used. The ratio between the applied strain rate and the relaxation time of the material is used to scale the elastoviscous rheology. The Deborah number (De) is the ratio of the stress magnitude to the elastic shear modulus (Reiner, 1964). De is lower than 10^{-4} for the layer and matrix in these models, representing a mechanical response close to the expected flow for an ideal viscous material (Poliakov and Hermann, 1994).

Results

Folding involving transversal asymmetry (A')

The effect of transversal asymmetry on fold shapes for periodic perturbations is examined in Fig. 5. All fold geometries correspond to a natural strain of $\varepsilon=0.8$ and can be compared with their initial shape (Fig. 3a; configurations with $\varphi=0$ and $-1 \leq A' \leq 1$). As expected, the fold shapes that develop are strongly controlled by the initial perturbation geometry. The increase of the parameter A' tends to generate an asymmetry across the layer. In such cases, differences on the geometry and curvature of external and internal hinges at both interfaces are observed. Hinges remain fixed at their initial material points during deformation and migrations or shifts of hinges during fold amplification are not observed. For the condition $A'=-1$, layer-parallel shortening is mainly accommodated by layer thickening and a slight amplification of the perturbation. This is agreement with the analytical solution, where low rates of dynamic amplification are observed (Fig. 4). After 70% shortening, the symmetry of the structure across and along the layer is still conserved and fold hinges remain aligned (Fig. 5, $A'=-1$). However, layer thickening is not homogenous at this point and is mainly accommodated at pinch regions. An increase of A' progressively produces structures similar to typical fold shapes, presenting reinforced amplification on both interfaces (*i.e.*, amplifications in the same direction) with an attenuation of layer thickness variations (Fig. 4). For all cases (except $A'=-1$) the final fold shapes are dominated by the lower interface. This clearly applies to the case of $A'=-0.5$, a model that starts with perturbations on both upper and lower interfaces with amplitude on opposite directions, but ends with reinforced amplitudes (Fig. 5). In models with $A'\leq0$, a marked difference in fold shapes between hinges located in swell and pinch regions is observed. Outer and inner arcs show smooth curvatures at swell areas

10

(Srivastava and Lisle, 2004). Additionally, pinch regions are characterised by high arc curvatures and shapes ranging between sinusoidal and hyperbolic. Differences in the amplification between both interfaces are observed, with the lowest A/H values measured at the upper interface of the layer. Note that these geometries resemble arc-and-cusp structures (e.g. Ramsay and Huber, 1987, p. 403), with strong hinge curvatures pointing at the lower amplified interface. The progressive amplification of the model $A'=0$ with only one horizontal interface) is shown in Fig. 6. In this model, hinge zones are fixed at the same material points during deformation, and the initial zones having maximum curvatures remain fixed at material points. In this case fold amplification is associated with the migration of inflexion points towards the inner hinges. The final geometry of the folding layer presents thickness variations, with pinch-and-swell regions being located at fold hinges and resulting in an asymmetry across the layer. In the early deformation stages, the differential stresses are higher at necking (or pinch) regions as a consequence of the thinner layer in these areas. However, progressive folding the layer-parallel stress field displays a typical distribution with high tensional stresses located along external fold arcs and compressional stresses at inner hinges.
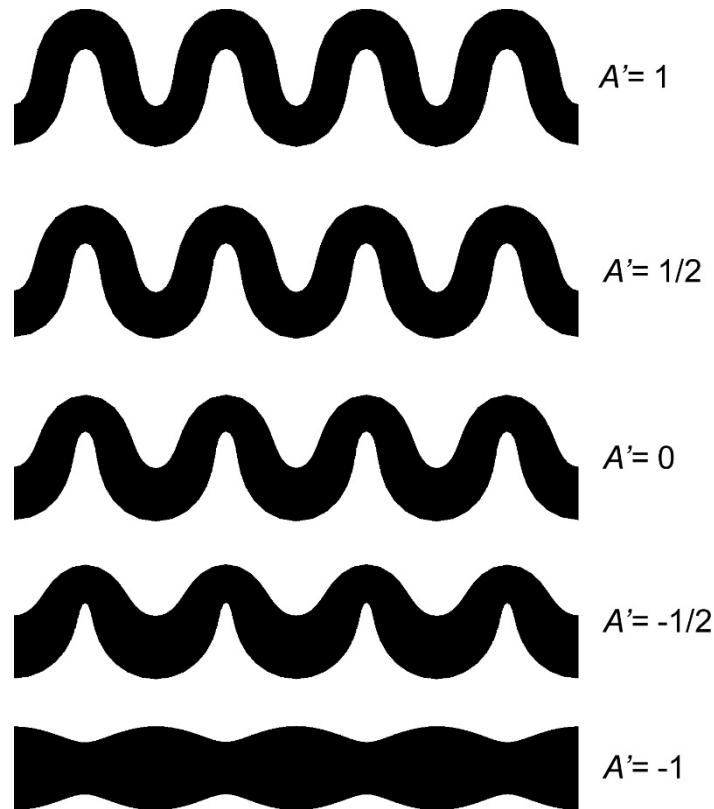

Figure 5. Influence of transversal asymmetry A' on the final shape of an array of periodic sinusoidal irregularities. Material properties are similar for all simulations and are listed in Table 1. The finite natural strain is $\varepsilon=0.8$.

The evolution of the averaged horizontal stress transversally to the layer in neck and pinch regions is showed in Fig. 7. With the exception of the $A'=-1$ case, all numerical simulations record a decrease of the averaged stress with increasing natural strain, in accordance with strain softening related to fold amplification (e.g., Schmalholz et al, 2005; Llorens et al., 2014). A marked stress relaxation occurs at pinch rather than at swell regions (e.g., model $A'=-0.5$). This larger structural softening of pinch regions in the models $A'=0$ and $A'=-0.5$ results in a stronger stress reduction compared to that in models with constant layer thickness ($A'=1$). Contrarily, the $A'=-1$ case maintains relatively large

values of the average stresses and non-homogeneous evolution. Regardless of the bulk softening or hardening, swell parts of the layer stiffen with progressive deformation while pinch portions soften. Therefore, a symmetric configuration of the perturbation geometry is associated with a nearly constant bulk horizontal stress at all deformation stages.
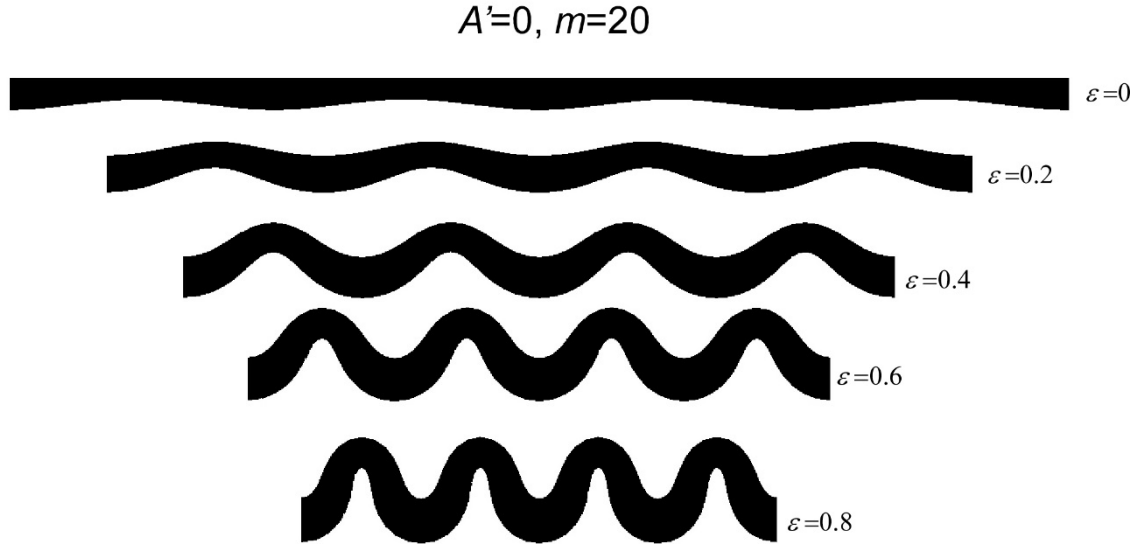
$$A'=0,\ m=20$$

Figure 6. Amplification of an initially periodic perturbation defined by *A'*=0 and viscosity contrast *m*=20. The upper interface of the layer was originally flat while the lower one presented a sinusoidal geometry. Differences on shape between hinges of upper and lower layer interfaces develop.

Models with an isolated perturbation at the centre of a single layer show a similar evolution than those with periodic perturbations (Fig. 8). However, the influence of transverse asymmetry on fold geometry is more evident. A progressive transition from "pure" fold shapes to folded swell regions is observed with decreasing *A'*. The model *A'*=-1 is the end-member case in which all shortening is accommodated by layer thickening. Except for *A'*=1, fold hinges are located at the thickening part of the layer. There is a weak tendency to develop and propagate lateral folds at the edges of swell regions. This is more relevant in models with -1<*A'*<0, in which the maximum strain localisation and fold amplification is observed on sideways folds (*e.g.*, model *A'*=-0.5 in Fig. 8). Additionally, in this range of models the maximum hinge curvatures are preferentially observed at outer fold arcs compared to the inner fold arcs. This observation contradicts the general tendency of folds of showing stronger curvatures along inner arcs (Hudleston and Lan, 1994; Huddleston and Treagus, 2010).

Folding involving longitudinal asymmetry (φ)

The influence of the longitudinal asymmetry (*φ*) on fold shape was investigated using periodic perturbations (Fig. 9) and isolated perturbations (Fig. 10). The shapes of the resulting folds show a marked variation with the parameter *φ*. The addition of a relative shift between the hinges of both interfaces produces the development of asymmetric folds (Fig. 9-10). This also applies to cases in which *φ* is small. For example, the perturbation in the model *φ*= π/32 is strong enough to induce an asymmetric folding, even if the hinge shifts are smaller than *d'*=0.03 units (Fig. 9). An increase of *φ* causes more intense fold amplification and a reduction of deformation accommodated by layer-parallel thickening. Although the initial wavelength is predefined as *L*=20, the initial hinge lateral shift

produces a variation of layer thickness thus causing differences in the initial wavelength to thickness ratio (L/H) between pinch and swell regions.

Figure 11 shows the evolution with shortening of the model with $\varphi = \pi/16$. During the first folding stages, hinges migrate and new wavelengths emerge (Fig. 11). The models tend to develop shorter wavelengths at pinch regions or thinned portions of the layer (L_{pinch} in Fig. 11 and $\varepsilon=0.8$), while longer wavelengths are observed at thicker zones of the layer (L_{swell} in Fig. 11 and $\varepsilon=0.8$). When limb dips attained values of 10° to 20°, hinge migration stops and hinges remain at the same position during further fold amplification. Differences on dip, length and layer thickness can be observed between both fold limbs (Figs. 10, 11). The final geometry is that of folded pinch-and-swell structures with a preferred location of swell zones at long limbs, while pinch regions are located at short fold limbs. A decrease of the parameter φ (Fig. 9) defines the transition between folds with symmetric ($\varphi=\pi/2$) and asymmetric limbs ($\pi/2<\varphi<0$). The wavelength of short limbs progressively decreases up to the end-member case of $\varphi=0$, where the short limb is only equivalent to the pinch region (Fig. 10).
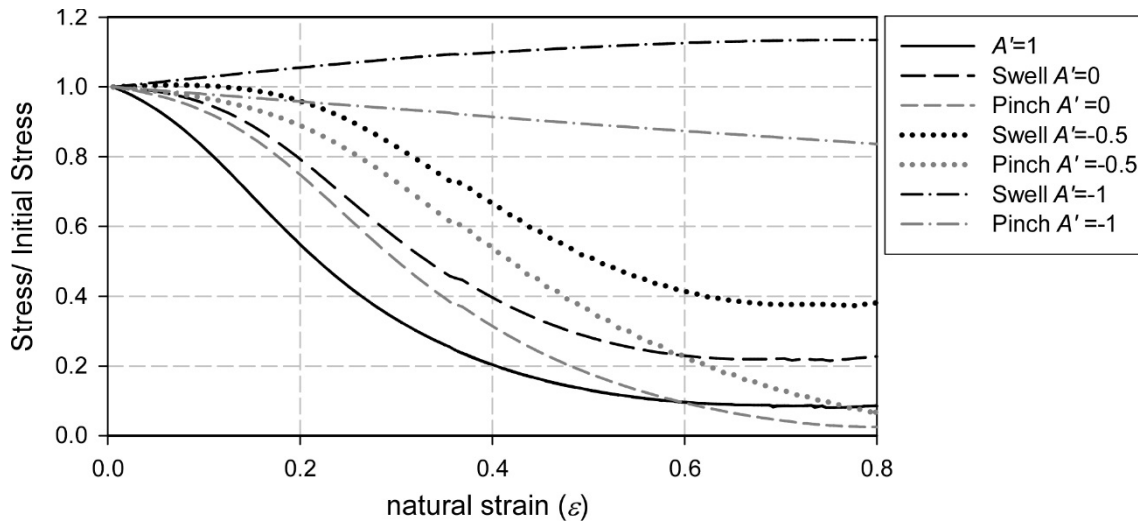

Figure 7. Evolution of the normalised averaged horizontal stress with natural strain (ε) at pinch and swell regions. All models were defined with transversal asymmetry between $A'=1$ and $A'=-1$. Except for the case $A'=-1$, the rest of the models show a marked reduction of stress with increasing strain. The grey and black curves indicate the pinch and swell regions, respectively. The averaged stress was normalised with respect to the initial stress (or membrane stress).

The influence of the parameter φ on the limb dip (α) of pinch and swell regions is shown in Fig. 12. For a constant φ value, pinch regions attain larger dips than swell regions. The highest dip values at swell regions increase with φ. However, this is not observed for pinch regions in which higher dip values are observed in intermediate models (*i.e.*, in between $\varphi=\pi/4$ and $\varphi=\pi/16$). The first derivative of limb dip change with respect to the natural strain ($\frac{\partial \alpha}{\partial \epsilon}$; "rotation rate") is showed in Fig. 12b with respect to the limb dip. This diagram provides an alternative way to analyse the influence of φ on fold growth rate. Limb rotation rates first increase and then decrease after attaining a maximum limb dip ranging between 20° and 40° (note that this applies for both positive and negative limb dips in Fig. 12). At low limb dips (-15 < α < 15°), the rotation rate is linear and independent of φ. This observation is coherent with Eq. (4) where the dynamic growth rate of a linear viscous material only depends on the viscosity contrast and wave number. However, when limb dips increase rotation rates become dependent on the longitudinal asymmetry φ. In general, the rotation rates at pinch regions are up to two or

three times higher than that observed at swell areas for the same φ configuration. For the case of $\varphi=0$, there is a thickening of the pinch-and-swell structure without growth of fold structures (*i.e.*, $\alpha=0$). Systematically, the values of rotation rates at swell zones are lower than in the $\varphi=\pi/2$ case (*i.e.*, antisymmetric case, where fold limbs are symmetric). However, rotation rates at pinch regions are higher than in the $\varphi=\pi/2$ case. The influence of increasing φ on fold limb rotation rates is not straightforward. In swell zones, an increase of the longitudinal asymmetry φ raises the rotation rate and displaces the peak of maximum rotation towards lower limb dip values. On the contrary, a direct relationship between φ and rotation rates is not observed in pinch regions (Fig. 12). The highest rotation rate values occur at intermediate values of φ in pinch regions. This is coherent with the peak displacement at higher limb dips.
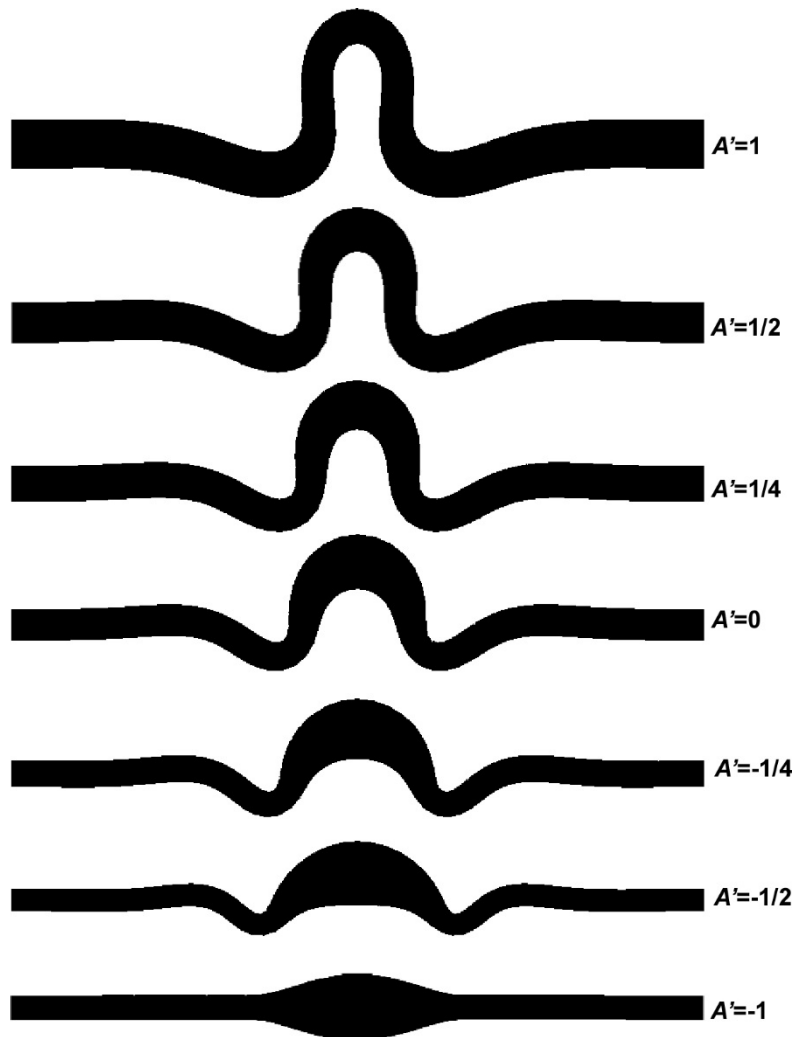

Figure 8. Influence of the parameter A' on the fold shape for planar layers defined with an initial, isolated perturbation at the centre of the layer. A gradual transition from both extremes can be observed. Increasing of A' enhances larger amplifications. In models with $A' < 0$, the final geometries resemble folded boudins, with lower curvatures in the inner arc compared to those in the outer arc. Sideway folds adjacent to the initial swell region develops in these models. The mechanical properties are the same for all simulations and are listed in Table 1. Final natural strain $\varepsilon=0.8$. Note that the scale is not the same in all the models.

These observations can be interpreted as consequence of the relative ratio between the wavelength to thickness (L/H) of pinch and swell regions with respect to the theoretical dominant wavelength to thickness ratio (L_d/H). For the case of a viscosity contrast of $m=20$, the initial $L/H=20$ used in the models is higher than the dominant

14

wavelength to thickness ratio (L_d/H =10). The introduction of the φ parameter produces a modification of the initial L. If we assume a layer with a constant thickness, the wavelength increase at swell zones produces higher L/H ratios than the initial ones, resulting in lower amplification rates (sees Fig. 3). Contrarily, a reduction of L at pinch areas results in a shorter L/H, which is close to the L_d/H value, and thus produces higher amplification rates.
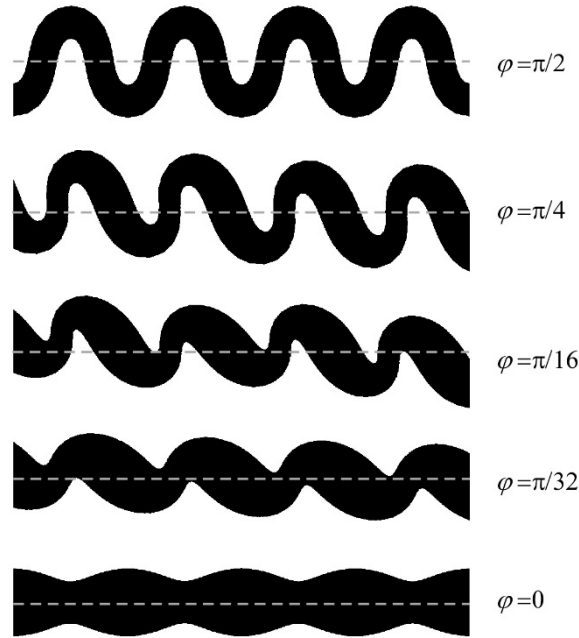

Figure 9. Influence of the initial longitudinal asymmetry (φ) of an array of periodic perturbations on the final geometry. General values of φ (*i.e.*, $0 < \varphi < \pi/2$) produce the development of asymmetric folds, with final arrangements defined by the preferred orientation of pinch and swell portions. Decreasing φ results in less amplifies folds and larger layer thickening. Natural strain ε=0.8. The dashed line indicates the initial layer envelope.
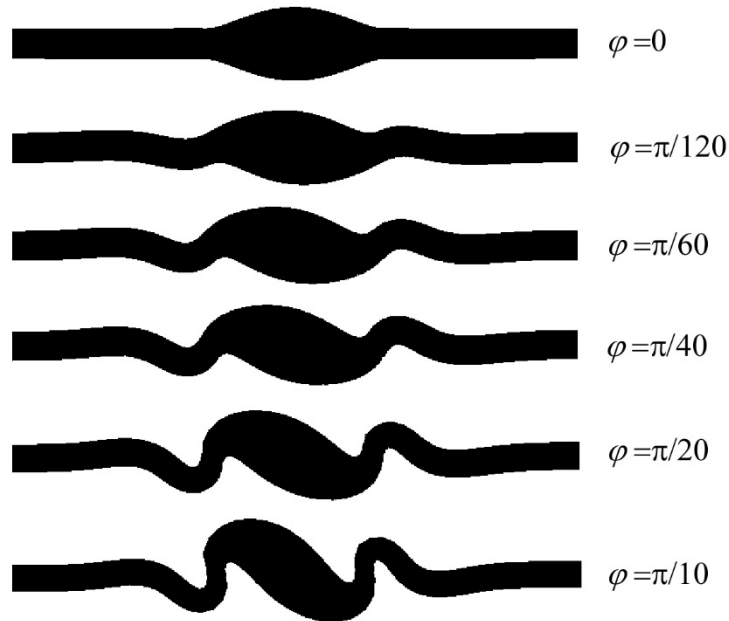

Figure 10. Comparison of the effect of the longitudinal asymmetry (φ) on folds developed in an initial flat layer with an isolated perturbation at the centre of it. Localisation of deformation tends to amplify side-wall folds near the margins of the swell areas. Note the sigmoidal geometry of folds with increasing φ, with swells located at the long fold limbs. Natural strain is ε=0.8 for all models.

Geometrical differences between folds located at the centre and edges of the model are detected, even if we have used periodic boundaries along the *x*-axis to minimize boundary effects (Fig. 9 and 11). Typically, folds in the centre of the model show less fold limb rotation but more thickening than folds at the edges. In models with longitudinal asymmetry ($\pi/2 < \varphi < 0$), a slight rotation of the layer envelope is observed, although the initial layer orientation was parallel to the shortening *x*-axis (Fig. 9). The sense of rotation of the layer envelope is the same as that of swell areas (or long limbs), and opposite to that of pinch zones (or short limbs), where larger dip limbs develop.

Models with an isolated perturbation (Fig. 8) present similar tendencies than those observed from simulations with periodic perturbations, although marked differences on final geometry can be observed. Deformation is strongly partitioned at the margin of the swell regions (*i.e.*, over-thickened parts of the layer) in models with isolated perturbations. In such cases, folds propagate on the sides of the swell. Deformation is preferentially accommodated by layer thickening in simulations with low longitudinal asymmetry φ, while increasing φ leads to a higher amplification and rotation of the swell zone. As in the case with periodic perturbations, the swell is located at the long and less rotated fold limb. However, the condition of free amplification and propagation of sideway folds reduces the final rotation of swells compared to the models with periodic perturbations. From a mechanical point of view it seems more efficient to propagate folds along the thin layer than deforming and rotating the over-thickened swell area. The last case would require a higher stress build-up. Layer envelopes do not rotate in isolated perturbation models.

Buckling involving transversal and longitudinal asymmetries

Figures 13 shows an example of fold amplification of a single layer with periodic perturbations defined by a combination of transversal (*A'*=-0.5) and longitudinal ($\varphi = \pi/16$) asymmetries. As expected attending to previous results, differences on fold shape across and along the layer envelope clearly influence the resulting fold trend. Remarkably, the developed folds display polarity, in a way that thick and thin fold hinges are preferentially located. This geometry is not a consequence of heterogenous layer deformation during folding, but reflects the initial perturbation geometry. At the final stage the hinges of the upper and lower layer interfaces are not aligned and, hence, fold axial planes show vergence with respect to the layer-envelope normal.

The influence of both types of asymmetries (*A'* and φ) on the final fold geometry is also explored for the case of an isolated layer perturbation (Fig. 14). All the models presented in this figure were carried out using a constant value of *A'*=-1/4, with the longitudinal asymmetry φ ranging between $\pi/120$ and $\pi/10$. The end-member case of φ=0 is shown in Fig. 8, illustrating the complexity of the finite fold geometries. A progressive geometrical transition is observed from a case in which the thick part of the layer corresponds to the hinge of an antiformal symmetric fold ($\varphi = \pi/120$) to a situation in which the thick part of the layer is folded and defines the hinge and limb of the developed fold ($\varphi = \pi/10$). In general, strong disharmonies of fold geometries with significant differences of curvature of fold hinges at both interfaces are developed. Although not displayed, axial plane orientations are highly variable in the matrix surrounding folds, with orientations from vertical attitudes in the case of pinched synformal hinges to sub-horizontal ones in the case of external arcs of antiformal swell portions.
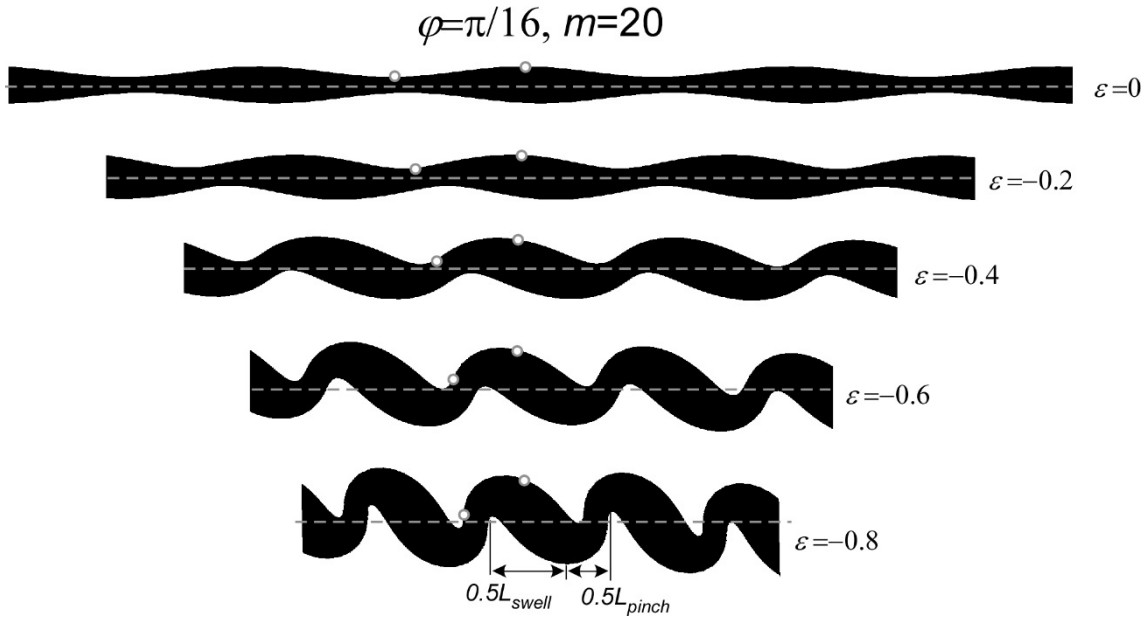
16

$$\varphi=\pi/16, \ m=20$$

$\varepsilon=0$

$\varepsilon=-0.2$

$\varepsilon=-0.4$

$\varepsilon=-0.6$

$\varepsilon=-0.8$

$0.5L_{swell}$ $0.5L_{pinch}$

Figure 11. Amplification of a periodic perturbation defined by $\varphi= \pi/16$. Circles indicate the location of the same material point (the initial point with maximum curvature) during different deformation stages. Hinge migration and selection of new wavelengths (shorter for pinch areas and larger for swell areas) can be observed during the first deformation stages. The dashed line indicates the initial layer envelope.

Discussion

Modelling of natural structures normally requires the simplification of observations in order to capture the key elements for understanding rock structure evolution (*e.g.*, Schmalholz, et al., 2008; Schmalholz and Mancktelow, 2016). For example, folds are generally described as periodic structures and geologists tend to study examples where regular fold trains are observed (*e.g.*, Ramsay and Huber, 1987; Hudleston and Treagus, 2010, their figs. 1-2). However, many natural folds are non-periodic structures with irregular distributions of wavelength and amplitude, and thus present variable fold geometries (*e.g.*, Fletcher and Sherwin, 1978; Hudleston and Holst, 1984; Abassi and Mancktelow, 1990, their fig. 3). Fold shapes are generally more variable in terranes affected by multiple deformation phases (Fig. 2a-c), in which there are layers with non-homogenous thickness and where pre-existing structures induce structural inheritance. These observations are coherent with experiments in which initial layer irregularities exert a strong influence on the final fold geometry (*e.g.*, Abbassi and Mancktelow, 1990; 1992). These authors observed that strongly asymmetric folds could develop from a small asymmetric perturbation despite the imposed layer-parallel shortening in pure shear conditions. Our numerical results reaffirm this interpretation. Fold shapes in all our simulations reflect the geometry of the initial perturbations. This is valid at least for elastoviscous materials in which the elastic response is low, as in the present case. For high-strain rate conditions ($d\varepsilon/dt=1e^{-10}$ s^{-1}), where build-up of stresses cannot be relaxed by viscous flow and where stresses can reach values of the order of GPa, it is possible that fold development is independent of the initial irregularities (Zhang et al. 2000, see their Fig. 9). However, such stresses are in general uncommon considering the properties of crustal rocks, and thus the material would fail by brittle or ductile strain localisation rather than being folded.
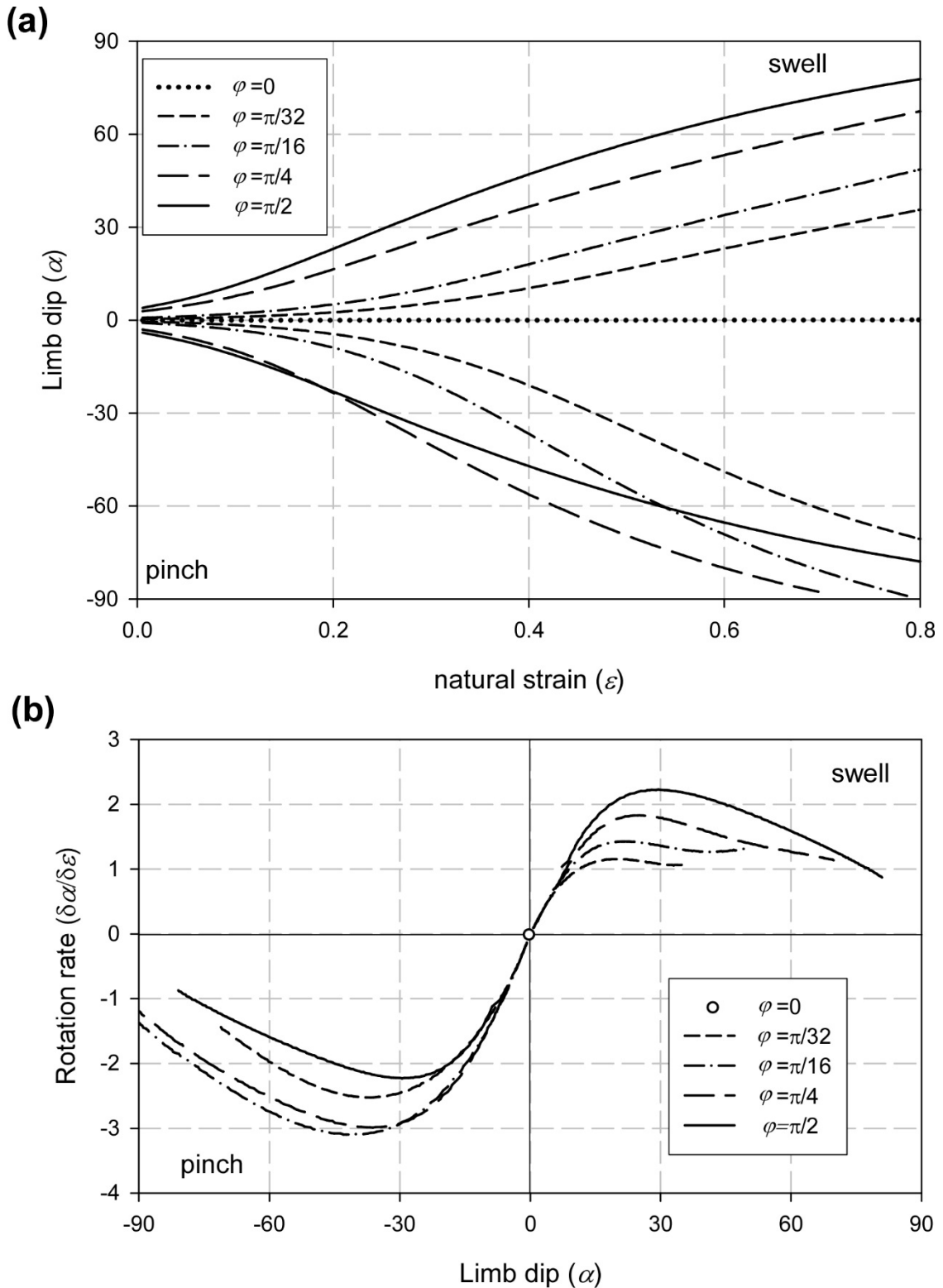
(a)

(b)

Figure 12. (a) Variation of the limb dip (α) with natural strain (ε). Positive values of α are used for swell regions, while negative values indicate pinch parts. A marked difference between pinch and swell limb dips can be observed, with the maximum rotation taking place at pinch regions. (b) Variation of the rotation rate of fold limbs ($\delta\alpha/\delta\varepsilon$) with respect to the limb dip (α) for models displayed in Fig.9. Positive values of α and $\delta\alpha/\delta\varepsilon$ are used for swells, while negative values correspond to pinch regions. For the model $\varphi=0$ pinch and swell regions do not rotate and data is equivalent to a point at the centre of the diagram.

The issue of structural inheritance is not restricted to small-scale structures as folds simulated in this study, but represents a multi-scale problem in structural geology

and tectonics. This issue has attracted attention from the large-scale tectonics community, as for example with the classical example of tectonic inversion of pre-rifted margins during a collision stage (*e.g.*, Butler et al., 2006, and references therein). Frequently, the geometry of thrust sheets and folded nappes developed in orogens are related to geometrical features of the pre-existing extensional basins, including their length, width or orientation with respect to the main reactivated faults (*e.g.*, von Tscharner et al., 2016). A direct application of our results to larger-scale tectonic problems is not straightforward due to the more complex material rheologies and the requirement to include gravity effects. Therefore, more advanced mechanical models are required to address similar problems at the crustal scale. However, our results are useful for illustrating the influence of inherited structures on the geometries of subsequent ones.

One of the aims of this study is to propose a simple approach to generalise the geometry of sinusoidal perturbations and use it to explore their influence on the geometry of the resulting folds. The definition of the two proposed geometrical parameters (*i.e.*, transversal asymmetry *A'* and longitudinal asymmetry *φ*) allows describing a wide spectrum of geometrical perturbations ranging between classical antisymmetric (or "fold shape") and symmetric (or "boudin shape") geometries. Any geometry in between the two end-members can be described with these two parameters, either in isolation or combing them (Fig. 3). Therefore from a geometrical point of view, pinch-and-swell geometries result a transition case between the two end members. The presence of transversal or longitudinal asymmetries along a layer results in the development of a directional polarity of the structure. For example, *A'* produces finite folds displaying differences on fold shapes between the upper and layer lower interfaces. For conditions of *A'*>0, upper and lower interfaces reflect the initial perturbations. However, in cases with *A'*<0 the initial geometry of one of the interfaces is not directly observable from the finite geometry of folds and yields anomalous geometries in which the curvature of inner arcs is lower than that outer arcs (Fig. 5 & 8). This contradicts the expected geometries of folds formed in viscous conditions from an initially flat layer (*e.g.*, Hudleston and Lan, 1994).

The folding of a layer with longitudinal asymmetry (summarised with the parameter *φ*) results in a systematic asymmetry of fold limbs and the formation of folds with vergence. Asymmetric folds are generally abundant in natural examples and are typically utilised to infer the sense of shearing. However, numerical simulations demonstrate that the development of asymmetries during folding is a critical issue. Results of single-layer folding simulations in simple shear conditions show that, in general folds, formed in such conditions present more or less symmetric geometries and are relatively similar to those formed under layer-parallel compression (Viola and Mancktelow, 2005; Llorens et al., 2013a). Numerical models also indicate that asymmetric folds only develop, and can be preserved with progressive deformation, in systems with a multi-layered matrix (Llorens et al., 2013b). Frehner and Schmalholz (2006) showed that the initial folds in multi-layered systems are symmetric, but the longer fold limbs rotate and small folds become asymmetric with progressive strain due to the relative shearing between fold limbs. Recently, Frehner and Schmid (2016) have shown that a pre-existing geometrical asymmetry can survive during multilayer folding, if the pre-existing perturbation is relatively tight and exhibits relatively high amplitudes. Otherwise flexural flow and flattening related to the longer fold limbs will result in de-amplification and unfolding. Asymmetric folds can probably also develop in systems with an anisotropic matrix and non-homogenous simple shear conditions (Ran et al., in review).

In any case, one of the ways to explain asymmetric folds is certainly based on the presence of initial systematic irregularities associated with primary structures (bedding and other stratigraphic surfaces, intrusive emplacement geometries, etc.) resulting in the formation of longitudinal asymmetries. In general, however, a systematic polarity of asymmetries is not expected in natural cases. Another option is that asymmetries arise from pre-existing deformation stages such as in terranes deformed in multiple tectonic phases. For example, an early phase of layer-parallel extension can produce a systematic development of initial irregularities that cause the development of fold asymmetries of folds during layer shortening in a subsequent deformation phase.

Although transversal and longitudinal asymmetries have been treated here as pre-existing geometries, there are mechanical processes that can induce their development with progressive deformation. For example, Gardner et al. (2015; 2016) showed that during extension of a viscous layer embedded in a matrix with different viscosities on the two sides of it (*i.e.*, in a tri-layer model), the pinch-and-swell or neck structures that develop present differences on amplitude between the upper and lower interfaces. Therefore, an effective way to develop a transversal anisotropy (*A'*) is by the presence of a viscosity contrast of materials surrounding the layer. Additionally, Gardner et al. (2015; 2016) demonstrated that asymmetric boudins can form by strain localisation and shearing. As shown by Duretz and Schmalholz (2015), this asymmetric shearing during layer-parallel extension is only effective for multi-layers if the material is power-law viscous. Accordingly, this phenomenon can dynamically produce longitudinal asymmetries, as those arising from numerical models, without requiring large amplitudes to induce asymmetries during subsequent folding. Finally, the emergence of systematic asymmetries under symmetric deformation conditions (as in cases of pure shear boundary conditions) has also recently been observed by Schöpfer et al (2017) in numerical simulations of faulting of layers subjected to layer-parallel extension. Domains with parallel faults with a systematically similar displacement sense form when the matrix surrounding the brittle layer has low strength. The formation and slip along parallel faults induces a fault-bonded block rotation of the layer to balance the vorticity components. A similar effect is observed in our simulations, as indicated in Fig. 9, with periodic sinusoidal perturbations with an initial longitudinal asymmetry. In our case the layer envelope rotates in the same sense than that of swell areas (or long limbs), and opposite to that of pinch zones (or short limbs), where larger rotations developed. Even if this phenomenon is in part influenced by model boundary effects, the layer envelope rotates to counteract the unbalanced vorticity originated by the final asymmetry of the folded array, attending to the initial orientation of the layer (*i.e.*, parallel to the shortening direction) and the coaxial boundary conditions, which present a theoretical vorticity of zero (*e.g.*, Lister and Williams, 1983).

Figures 2c-d show examples of folded quartz veins hosted in schists from the Cap de Creus Variscan Belt (Spain). Folds present complex shapes and display irregular layer thickness distributions. These folds were interpreted to have formed by two different deformation phases (Carreras and Druguet, 1994). An early extension parallel to quartz veins and schists produced the development of boudinage, pinch-and-swell structures and heterogeneous layer thickness of quartz veins. During a subsequent deformation phase, quartz veins were folded. Some of the fold geometries resemble those obtained from the numerical models presented here, although natural patterns are more complex than those in our simulations. For example, the asymmetric arrangement of boudins and preferred rotation of pinch parts with respect to boudins is in agreement with the presence of an

initial longitudinal asymmetry (see Fig. 2a-c). Moreover, folded swell portions, localisation of folds at boudin margins and folds with smoothed inner arcs are indicative of the presence of initial layers that already had strong thickness variations. However, a systematic variation compatible with a transversal asymmetry (*i.e.*, a transverse polarity in folds) is not observed in this field example. The early deformation phase may have be produced an asymmetric boudinage of the rocks. This boudinage would have pre-determined the geometry of the amplified folds developed during the layer-parallel shortening phase. Alternatively, asymmetric folds can be explained as a result of deformation with a sinistral sense of shear parallel to the layers during shortening (Druguet et al., 1997). Assessing the suitability of either a kinematic interpretation, or providing an explanation based on the arrangement of initial layer interface perturbations, requires a more extensive study of the geometries of these structures in the field area. However, in this case both deformation kinematics and initial perturbations probably influenced the final structure. However, numerical simulations demonstrate that during pure shear deformation of a stiff layer parallel to the shortening direction, asymmetric structures can develop as a consequence of the initial shape of layer irregularities, without implying non-coaxial deformation. The use of multiple kinematic indicators can help to constraint the sense of shear, but it is critical to take into account that discrepancies between kinematic indicators and fold asymmetry may be due to the systematic influence of the geometry of initial perturbations.

The generalisation of perturbation geometries illustrates well the problem of folding of layers with non-homogenous thickness. A simple and idealised case represents the folding of a pre-existing pinch-and-swell structure. It is worth noting that our analysis is restricted to a limited spectrum of the possible range of initial perturbations. Our numerical simulations were carried out using constant wavelength between pinch and swell regions and a linear elasto-viscous behaviour. However, there is a much wider field of initial settings to be explored, including variable layer length ratios or different thickness ratios between pinch and swell regions. Additionally, if a power-law viscous rheology is considered the strain localisation pattern and fold amplification behaviour would be more intense (*e.g.*, see Llorens et al., 2013a; Ran et al., in review). A systematic analysis is beyond the scope of this paper, but the results presented here are a start point to promote further investigations on the influence of non-homogenous layer thickness on fold development.

Finally, and returning to the "fish-hook" folds of Ramsay and Huber (1983), our results can be used for reinterpreting non-periodic folds with irregular distributions of wavelength and amplitude. As described in the introduction, a unique feature of "fish-hook" folds is that they present a marked geometric polarity, with differences in fold hinge geometry between the upper and lower layer interfaces. The latter authors proposed an interpretation of "fish-hook" structures based on a tri-layer system, where matrix above and below the competent layer have different viscosities. During non-coaxial deformation, the viscosity contrast between layer and matrix induces distinct wavelength selection along the upper and lower interfaces of the layer (see Fig. 17.18 of Ramsay and Huber, 1983). A simpler explanation is that the structure is derived from folding of a pinch-and-swell structure with longitudinal and transversal asymmetry. Note the similarity between the models $\phi=\pi/16$ showed in Fig. 13 and $\phi=\pi/10$ in Fig. 14, with the geometry of "fish-hook" structures in Fig. 1.

$A' = -1/2, \varphi = \pi/16, m = 20$

$\varepsilon = 0$

$\varepsilon = -0.2$

$\varepsilon = -0.4$

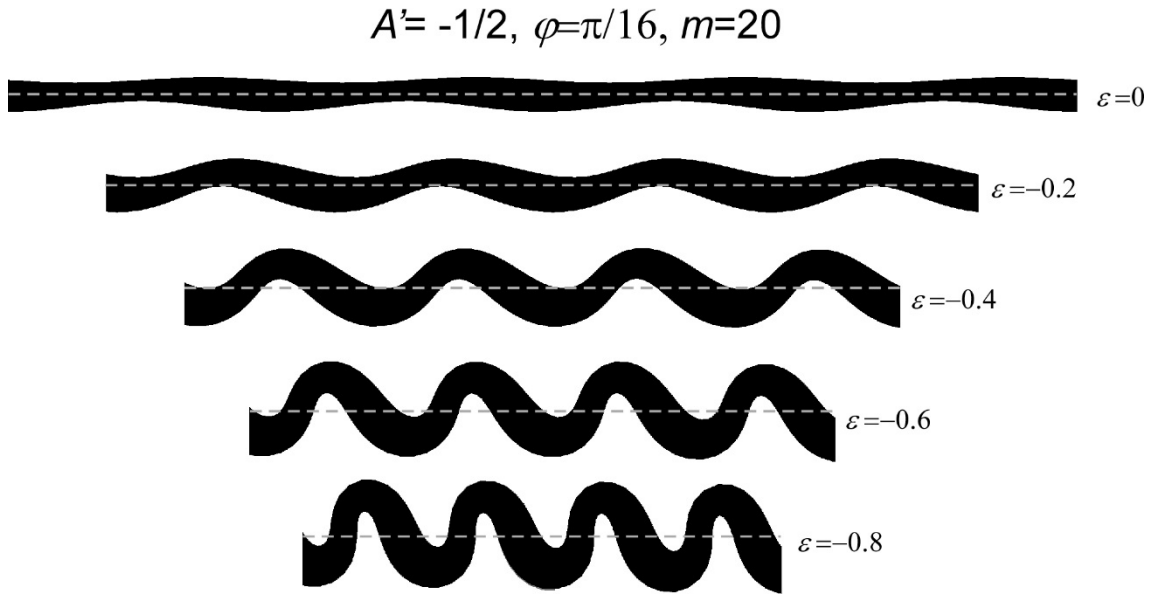$\varepsilon = -0.6$

$\varepsilon = -0.8$

Figure 13. Amplification of a periodic perturbation defined by longitudinal and transversal asymmetries ($\varphi = \pi/16$ and $A' = -1/2$). The final folds show differences on hinge thickness across the layer and asymmetries along the layer envelope. The dashed line indicates the initial layer envelope.
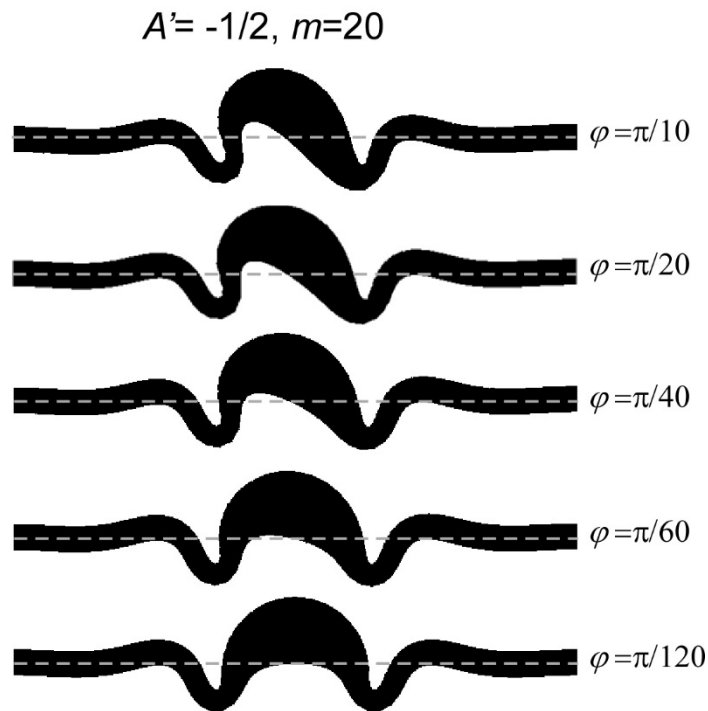
$A' = -1/2, m = 20$

$\varphi = \pi/10$

$\varphi = \pi/20$

$\varphi = \pi/40$

$\varphi = \pi/60$

$\varphi = \pi/120$

Figure 14. Example of the influence of the parameter φ on fold shapes in a model defined by a single isolated perturbation with constant $A' = -1/4$. Increasing φ produces a gradual transition between models where the swell areas define the hinge of an antiform ($\varphi = \pi/120$), to cases in which swell areas are in fold limbs ($\varphi = \pi/10$). Natural strain is $\varepsilon = 0.8$. Layers are turned to show the same asymmetry sense than in Fig. 1a. Note the similarity of folds with $\varphi = \pi/10$ and the "fish-hook" folds of Ramsay and Huber (1987) (see Fig. 1).

Conclusions

We have investigated the effect of the initial layer interface geometry on single-layer folding by means of numerical simulations. The geometry of a periodic or isolated sinusoidal perturbation has been generalised using two shape parameters, namely transversal asymmetry A' and longitudinal asymmetry φ. In this way, we can study the gradual transition between the two-classical end-member fold geometries (*i.e.*, symmetric and antisymmetric). These parameters describe the initial variation of layer thickness, with thickened layer regions (*i.e.*, swell) and thinned layer parts (*i.e.*, pinch). During layer-parallel shortening, the initial perturbation geometry strongly controls the finite amplitude and geometry of resulting folds. These parameters can describe a directional polarity of the resulting folds, either along or across the layer. Increasing these parameters enhances fold amplification. In the case of transversal asymmetry, the results indicate that the upper and lower fold interfaces can exhibit different shapes and curvature can thus differ along consecutive fold hinges. However, variation of layer thickness tends to be compensated. Models ranging between $-1<A'<0$ are the exception case, because the initial geometry of one of the interfaces is not directly observable from finite folds and yields anomalous geometries where curvatures of inner arcs are lower than those of outer arcs. In the case of longitudinal asymmetries a preferential arrangement of pinch and swell regions develops, with variations of wavelength and dip along consecutive fold limbs. In general, thin and short limbs (*i.e.*, pinch portions) rotate faster than thick and long ones (*i.e.*, swell portions) and produce a variation of wavelength and dip along consecutive limbs. Migration of hinge points with respect to the initial perturbation geometry takes place during the first folding stages and is required to accommodate wavelength selection. Despite the limitations of numerical simulations, in which an idealised and sinusoidal perturbation is utilised, the results can be qualitatively used to better understand irregular and non-periodic natural fold patterns, and improve structural analysis. Our study illustrates the influence of inherited structures on the geometries of folds developed in successive tectonic phases, and demonstrates that caution must be taken when using asymmetric folds for strain analysis and as kinematic indicators.

Acknowledgements

References

Abbassi, M. R. and Mancktelow, N. S. 1990. The effect of initial perturbation shape and symmetry on fold development. *Journal of Structural Geology*, **12**, 273–282.

Abbassi, M. R. and Mancktelow, N. S. 1992. Single layer buckle folding in non-linear materials-I: Experimental study of fold development from an isolated initial perturbation. *Journal of Structural Geology*, **14**, 85–104.

Biot, M. A. 1957. Folding instability of a layered viscoelastic medium under compression. *P. Roy. Soc. Lond. A*, **242**, 444–454.

Biot, M. A. 1959. Folding of a layered viscoelastic medium derived from an exact stability theory of a continuum under initial stress. *Applied Mathematic Q.*, **17**, 185-204.

Biot, M. A. 1961. Theory of folding of stratified viscoelastic media and its implications in tectonics and orogènesis. *Geol. Soc. Am. Bull.,* **72**, 1595–1620.

Burg, J.-P., Kaus B.J.-P. & Podladchikov, Y.Y. 2004. Dome structures in collision orogens: Mechanical investigation of the gravity/compression interplay, in Whitney D.L. et al. eds., Gneiss domes in orogeny: Geological Society of America Special Paper 380, p. 47 – 66.

Butler, R. B., Tavarnelli, E. & Grasso, M. 2006. Structural inheritance in mountain belts: An Alpine-Apennine perspective. *Journal of Structural Geology*, **28**, 1893-1908.

Carreras, J. & Druguet, E. 1994. Structural zonation as a result of inhomogeneous non-coaxial deformation and its control on syntectonic instrusions: an example from the Cap de Creus area (eastern-Pyrenees). *Journal of Structural Geology*, **16**, 1525-1534.

Cobbold, P. R. 1975. Fold propagation in single embedded layers. *Tectonophysics*, **27**, 333–351.

Cundall, P.A. and Board, M. 1988. A microcomputer pro- gram for modelling large-strain plasticity problems. In: G. Swoboda (Editor), Numerical Methods in Geomechanics. Balkerna, Rotterdam, pp. 2101-2108.

Druguet, E., Passchier, C.W., Carreras, J., Victor, P. & den Brok, S. 1997. Analysis of a complex high-strain zone at Cap de Creus, Spain. *Tectonophysics*, **280**, 31-45.

Duretz, T. & Schmalholz, S. M. 2015. From symmetric necking to localized asymmetric shearing: The role of mechanical layering. *Geology*, **43**, 711–714.

Fletcher, R. C. 1974. Wavelength selection in the folding of a single layer with power-law rheology. *American Journal of Science*, **274**, 1029–1043.

Fletcher, R. C. 1991. 3-Dimensional folding of an embedded viscous layer in pure shear. *Journal of Structural Geology*, **13**, 87–96.

Fletcher, R.C. 1995. 3-dimensional folding and necking of a power-law layer – are folds cylindrical, and, if so, do we understand why?. *Tectonophysics*, 247, 65–83.

Fletcher, R. C. & Sherwin, J. 1978. Arc lengths of single layer folds: a discussion of the comparison between theory and observations. *American Journal of Science*, **274**, 1029-1043.

Frehner, M. & Schmalholz, S. M. 2006. Numerical simulations of parasitic folding in multilayers, *Journal of Structural Geology*, **28**, 1525-1534.

Frehner, M. & Schmid, T. 2016. Parasitic folds with wrong vergence: How pre-existing geometrical asymmetries can be inherited during multilayer buckle folding. *Journal of Structural Geology*, **87**, 19-29.

Gardner, R. L., Piazolo, S. & Daczko, N. R. 2015. Pinch and swell structures: evidence for strain localisation by brittle–viscous behaviour in the middle crust. *Solid Earth*, **6**, 1045–1061.

Gardner, R. L., Piazolo, S. & Daczko, N. R. 2016. Shape of pinch and swell structures as a viscosity indicator: Application to lower crustal polyphase rocks. *Journal of Structural Geology*, **88**, 32-45.

Gomez-Rivas, E., Griera, A., Llorens, M.-G., Bons, P.D., Lebensohn, R. & Piazolo, S. 2017. Subgrain rotation recrystallization during shearing: insights from full-field numerical simulations of halite polycrystals. *Journal of Geophysical Research Solid Earth*, **122 (11)**, 8810-8827.

Goscombe B. D. & Passchier C. W. 2003. Asymmetric boudins as shear sense indicators – an assessment from field data. *Journal of Structural Geology*, **25**, 575–9589.

Hudleston, P. J. & Holst, T. B. 1984. Strain analysis and fold shape in limestone layer and implications for layer rheology. *Tectonophysics*, **106**, 321-347.

Hudleston, P. J. & Lan, L. 1994. Rheological controls on the shapes of single-layer folds. *Journal of Structural Geology*, **16**, 1007-1021.

Hudleston, P. J. & Treagus, S. H. 2010. Information from folds: A review. *Journal of Structural Geology*, **32**, 2042–2071.

Itasca Consulting Group Inc. 1998. FLAC: Fast Lagrangian Analysis of Continua, Optional Features, version 3.4. Itasca Consulting Group Inc, Minneapolis.

James, A. I. & Watkinson, A. J. . 1994. Initiation of folding and boudinage in wrench shear and transpression. *Journal of Structural Geology*, **16**, 883-893.

Jessell, M.W., Bons, P.D., Griera, A. & Evans, L. 2009. A tale of two viscosities. *Journal of Structural Geology*, **31**, 719–736.

Johnson, A. M. & Fletcher, R. C. 1994. Folding of Viscous Layers, Columbia University Press, New York.

Lan, L. & Hudleston, P.J., 1991. Finite-element models of buckle folds in non-linear materials. *Tectonophysics*, **199**, 1-12.

Lister, G. S. & Williams, P. F. 1983. The partitioning of deformation in flowing rock masses. *Tectonophysics*, **92**, 1-33.

Llorens, M.-G., Bons, P. D., Griera, A., Gomez-Rivas, E. & Evans, L. A. 2013a. Single layer folding in simple shear. *Journal of Structural Geology*, **50**, 209–220.

Llorens, M.-G., Bons, P. D., Griera, A. & Gomez-Rivas, E. 2013b. When do folds unfold during progressive shear? *Geology*, **41**, 563–566.

Llorens, M.-G., Bons, P. D., Griera, A. & Gomez-Rivas, E. 2014. Mechanics of fold development in pure- and simple shear. In: Pardo-Igúzquiza E., Guardiola-Albert C., Heredia J., Moreno-Merino L., Durán J., Vargas-Guzmán J. (eds) Mathematics of Planet Earth. Lecture Notes in Earth System Sciences. Springer, Berlin, Heidelberg.

Mancktelow, N. S. 1999. Finite-element modelling of single-layer folding in elasto-viscous materials: the effect of initial perturbation geometry. *Journal of Structural Geology*, **21**, 161–177.

Poliakov, A. N. B. & Hermann, H. J. 1994. Self-organized criticality of plastic shear bands in rocks. *Geophysical Research Letters*, 21 (19), DOI: 10.1029/94GL02005.

Ramberg, H. 1960. Relationship between length of arc and thickness of ptygmatically folded veins. *American Journal of Science*, **258**, 1595-1620.

Ramsay, J. G. 1967. Folding and Fracturing of Rocks, McGraw-Hill, New York.

Ramsay, J. G. & Huber, M. I. 1987. The Techniques of Modern Structural Geology, Volume 2: Folds and Fractures, Academic Press, London.

Ran, H., de Riese, T., Llorens, M.-G., Finch, M., Evans, L. A., Gomez-Rivas, E., Griera, A., Jessell, M. W., Lebensohn, R. A., Piazolo, S. & Bons, P. D. (in press). Time for anisotropy: The significance of mechanical anisotropy for the development of deformation structures. *Journal Structural Geology*.

Ranalli, G. 1987. Rheology of the Earth. Allen and Unwin. Boston.

Reiner, M. 1964. The Deborah number. *Physics Today*, 17, 62. http://dx.doi.org/10.1063/1.3051374

Schmalholz, S. M. & Mancktelow, N. S. 2016. Folding and necking across the scales: a review of theoretical and experimental results and their applications. *Solid Earth*, **7**, 1417-1465.

Schmalholz, S. M. & Podladchikov, Y. 1999. Buckling versus folding: Importance of viscoelasticity, *Geophysical Research Letters*, **26**, 2641–2644.

Schmalholz, S. M. & Podladchikov, Y. Y. 2000. Finite amplitude folding: transition from exponential to layer length controlled growth. *Earth Planetary Science Letters*, **181**, 617–633.

Schmalholz, S. M. & Podladchikov, Y. Y. 2001. Strain and competence contrast estimation from fold shape. *Tectonophysics*, **340**, 195– 213.

Schmalholz, S. M., Podladchikov, Y. Y. & Jamtveit, B. 2005. Structural softening of the lithosphere. *Terra Nova*, **17**, 66–72.

Schmalholz, S. M., Schmid, D.W. & Fletcher, R. C. 2008. Evolution of pinch-and-swell structures in a power-law layer. *Journal of Structural Geology*, **30**, 649–663.

Schöpfer, M. P. J., Childs, C., Manzocchi, T., Walsh, J. J., Nicol, A. & Grasemann, B. 2017. The emergence of asymmetric normal fault systems under symmetric boundary conditions. . *Journal of Structural Geology*, **104**, 159-171.

Smith, R. B. 1975. Unified theory of the onset of folding, boudinage, and mullion structure. *Geological Society American Bulletin*, **86**, 1601–1609.

Smith, R. B. 1977. Formation of folds, boudinage, and mullions in non-Newtonian materials. *Geological Society American Bulletin*, **88**, 312–320.

Smith, R. B. 1979. The folding of a strongly non-newtonian layer. *American Journal of Science*, **279**, 272–287.

Sokoutis, D. 1987. Finite strain effects in experimental mullions. *Journal of Structural Geology*, **9**, 233-242.

Sokoutis, D. 1990. Experimental mullions ay single and double interfaces. *Journal of Structural Geology*, **12**, 365-373.

Sorby, H. C. 1879. The structure and origin of limestones. *J. Geol. Soc. London Proceedings*, **35**, 56-93.

Srivastava, D, P. & Lisle, R. J. 2004. Rapid analysis of fold shape using Bézier curves. *Journal of Structural Geology*, **26**, 1553-1559.

Swanson, M. T. 1992. Late Acadian-Alleghenian transpressional deformation: evidence from asymmetric boudinage in the Casco Bay area, coastal Maine. *Journal of Structural Geology*, **14**, 323-341.

Takeda, Y-T. & Griera, A. 2006. Rheological and kinematical responses to flow of two-phase rocks. *Tectonophysics*, **427**, 95-113.

Toimil, N. C. & Griera, A. 2007. Influence of viscosity contrast and anisotropy on strain accommodation in competent layers. *Journal of Structural Geology*, **29**, 787-801.

Turcotte, D. L. & Schubert, G. 1982. Geodynamics. Applications of continuum physics to geological problems. John Wiley and Sons, New York.

Viola, G. & Mancktelow, N. S. 2005. From XY tracking to buckling: axial plane cleavage fanning and folding during progressive deformation. *Journal of Structural Geology*, **27**, 409-417.

von Tscharner, M., Schmalholz, S. M. & Epard, J.-L. 2016. 3-D numerical models of viscous flow applied to fold nappes and the Rawil depression in the Helvetic nappe System (western Switzerland). *Journal of Structural Geology*, **86**, 32-46.

Williams, P. F. & Jiang, D. 2001. The role of initial perturbations in the development of folds in a rock-analogue. *Journal of Structural Geology*, **23**, 843-856.

Williams, J. R., Lewis, R. W. & Zienkiewicz, O. C. 1978. A finite-element analysis of the role of initial perturbation in the folding of a single viscous layer. *Tectonophyscis*, **45**, 187-200.

Zhang, Y., Hobbs, B., Ord, A. & Mühlhaus, H. 1996. Computer simulation of single-layer buckling. *Journal of Structural Geology*, **18**, 643–655.

Zhang, Y., Mancktelow, N. S., Hobbs, B., Ord, A. & Mühlhaus, H. 2000. Numerical modelling of single-layer folding: clarification of an issue regarding the possible effect of computer codes and the influence of initial irregularities. *Journal of Structural Geology*, **22**, 1511–1522.